A Global Simulation Study of ICRF Heating by TASK/WM and GNET in Toroidal Plasmas

Tetsuya YAMAMOTO, Sadayoshi MURAKAMI and Atsushi FUKUYAMA

Department of Nuclear Engineering, Kyoto University, Kyoto 606-8501, Japan

(Received: 1 September 2008 / Accepted: 9 January 2009)

A global simulation code is developed to study the ICRF heating combining two global simulation codes: a full wave field solver, TASK/WM, and a drift kinetic equation solver, GNET. The both codes can treat a 3-D magnetic configuration based on the MHD equilibrium by VMEC code. The developed code is applied to the ICRF minority heating in a simple circular tokamak. The ICRF wave propagation is solved by TASK/WM and the obtained RF electric field is used to solve the drift kinetic equation by GNET. The analyses are carried out in the on and off axis heating cases. The characteristics of energetic ion distribution in the phase space are investigated. It is found that an asymmetry in the parallel velocity distribution appears due to the finite orbit width effect and that the asymmetry direction depends on the minor radius position.

Keywords: ICRF heating, Simulation

1. Introduction

The ion cyclotron range of frequencies (ICRF) heating has long been considered a primary plasma heating method. The physics basis and the efficiency of ICRF heating have been confirmed by experimental, theoretical and simulation studies. However, there still remains several important issues in ICRF heating, e.g. finite orbit effect of energetic ions, current drive, toroidal flow generation, etc. In order to clarify these problems, a global simulation study which takes into account the wave-plasma interaction self-consistently is necessary.

In this paper, we study the ICRF heating in toroidal plasmas by combining two global simulation codes: a full wave field solver TASK/WM [1] and a drift kinetic equation solver GNET [2], as a first step to develop a self-consistent simulation. The realistic ICRF wave profile obtained by TASK/WM is used to solve a drift kinetic equation by GNET. The both codes can treat a 3-D magnetic configuration based on the MHD equilibrium by VMEC code.

In Sec. 2 the simulation models and codes are described and, then, simulation results are presented in Sec. 3. Finally, the obtained results are summarized in Sec. 4.

2. Simulation model

In this study we combine two simulation code to study the ICRF heating. The simulation model is illustrated in Fig. 1. First, Maxwell's equation for RF wave is solved by TASK/WM code, then the obtained RF wave electric field profile is used to solve a drift kinetic equation by GNET code. Finally, the steady state velocity distribution function of plasma is obtained.

author's e-mail: yamamoto@p-grp.nucleng.kyoto-u.ac.jp

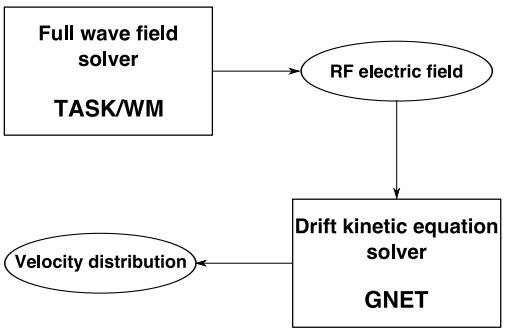

Fig. 1 The schematic diagram of simulation model

TASK/WM code solves Maxwell's equation for RF wave electric field, $\boldsymbol{E}$, with complex frequency, ω,

$$\nabla \times \nabla \times \boldsymbol{E} = \frac{\omega^2}{c^2} \overleftrightarrow{\epsilon} \cdot \boldsymbol{E} + i\omega\mu_0 \boldsymbol{j}_{\rm ext}, \tag{1}$$

where the external current density, $\boldsymbol{j}_{\rm ext}$ denotes the antenna current in ICRF heating, as a boundary value problem in the 3-D magnetic configuration. In the present analysis, a simple collisional cold plasma model is applied [3]. Maxwell's equation Eq. (1) is formulated by expansion to Fourier mode in poloidal and toroidal direction and finite different method in radial direction. Then the electric field is formulated as

$$\boldsymbol{E}(\psi_l, \theta, \varphi) = \sum_{mn} \boldsymbol{E}_{mn}(\psi_l) e^{i(m\theta + n\varphi)}, \tag{2}$$

where l, m, n are the radial grid number, poloidal and toroidal mode numbers, respectively.

GNET code solves a linearized drift kinetic equation for energetic ions including complicated behavior

of trapped particles in 5-D phase space as

$$\frac{\partial f}{\partial t} + (\boldsymbol{v}_\parallel + \boldsymbol{v}_\mathrm{D}) \cdot \nabla f + \boldsymbol{a} \cdot \nabla_{\boldsymbol{v}} f - C(f) - Q_\mathrm{ICRF}(f) - L = S, \quad (3)$$

where $C(f)$ and Q_ICRF are the linear Coulomb collision operator and the ICRF heating term, respectively. S and L are the particle source term by ionization of neutral particles and sink (loss) term including orbit loss and charge exchange, respectively.

In order to solve the linearized drift kinetic equation (3) by Monte Carlo method, the Green function, $\mathcal{G}$, is introduced as

$$\frac{\partial \mathcal{G}}{\partial t} + (\boldsymbol{v}_\parallel + \boldsymbol{v}_\mathrm{D}) \cdot \nabla \mathcal{G} + \boldsymbol{a} \cdot \nabla_{\boldsymbol{v}} \mathcal{G} - C(\mathcal{G}) - Q_\mathrm{ICRF}(\mathcal{G}) - L = 0 \quad (4)$$

with the initial condition $\mathcal{G}(\boldsymbol{x}, \boldsymbol{v}, t = 0 | \boldsymbol{x}', \boldsymbol{v}') = \delta(\boldsymbol{x} - \boldsymbol{x}')\delta(\boldsymbol{v} - \boldsymbol{v}')$. The $\mathcal{G}$ is evaluated by solving the equation of motion for guiding center of test particles expressed by the Hamiltonian of charged particle

$$H = \frac{1}{2} m v_\parallel^2 + \mu B(\psi, \theta, \varphi) + q\Phi(\psi) \quad (5)$$

in Boozer coordinate. In order to solve the equation of motion, 6th-order Runge-Kutta method is applied. The collisional effects are taken into account using the linear Monte Carlo collision operator [4].

The ICRF heating term is modelled by changing the perpendicular velocity of the test particle passing through the resonance layer, $\omega - k_\parallel v_\parallel = n\Omega$, by

$$\begin{aligned}\Delta v_\perp \approx & \left[\left(v_{\perp 0} + \frac{q}{2m} I |E_+| J_{n-1}(k_\perp \rho) \cos\phi_\mathrm{r} \right)^2 \right. \\ & \left. + \frac{q^2}{4m^2} \left\{ I |E_+| J_{n-1}(k_\perp \rho) \right\}^2 \sin^2 \phi_\mathrm{r} \right]^{-\frac{1}{2}} \\ & - v_{\perp 0} \\ \approx & \frac{q}{2m} I |E_+| J_{n-1}(k_\perp \rho) \cos\phi_\mathrm{r} \\ & + \frac{q^2}{8m^2 v_{\perp 0}} \left\{ I |E_+| J_{n-1}(k_\perp \rho) \right\}^2 \sin^2 \phi_\mathrm{r}, \end{aligned} \quad (6)$$

where E_+ and ϕ_r are the left-circularly polarized component of RF wave electric field and random phase, respectively. Also, q, m, ρ, J_n are the charge, mass, the Larmor radius of the particle and nth Bessel function, respectively. The time duration passing through the resonance layer, I, is given by the minimum value as, $I = \min(\sqrt{2\pi/n\dot{\Omega}}, 2\pi(n\ddot{\Omega})^{-1/3}\mathrm{Ai}(0))$, which corresponds to two cases; the simple passing of the resonance layer and the passing near the turning point of a trapped motion (banana tip).

In the simulation $|E_+|$ evaluated by TASK/WM is used in Eq. (6). We consider only fundamental ion cyclotron resonance and assume $k_\perp \rho$ is small in this study. Therefore,

$$|E_+| J_{n-1}(k_\perp \rho) \approx |E_+|. \quad (7)$$

Assuming $B_\varphi \gg B_\theta$, $k_\parallel$ is evaluated as

$$k_\parallel \approx \frac{n}{R}, \quad (8)$$

where n is the toroidal mode number in Eq. (2) and R is the major radius.

Finally the velocity distribution function is calculated by integrating the particle in the phase space over initial position $(\boldsymbol{x}', \boldsymbol{v}')$ and initial time t' as

$$f(\boldsymbol{x}, \boldsymbol{v}, t) = \int_0^t dt' \int d\boldsymbol{x}' \int d\boldsymbol{v}' S\, \mathcal{G}(\boldsymbol{x}, \boldsymbol{v}, t - t' | \boldsymbol{x}', \boldsymbol{v}'). \quad (9)$$

3. Simulation results

We study the ICRF minority heating applying the developed code in the simple tokamak plasma. The cross section of the MHD equilibrium by VMEC code are shown in Fig. 2. The plasma parameters are listed in Table 1. The magnetic axis of this plasma shifts to the outer side of the plasma due to the finite β effect (Fig. 2). We assume deuterium (D) as a majority ion and hydrogen (H) as a minority ion.

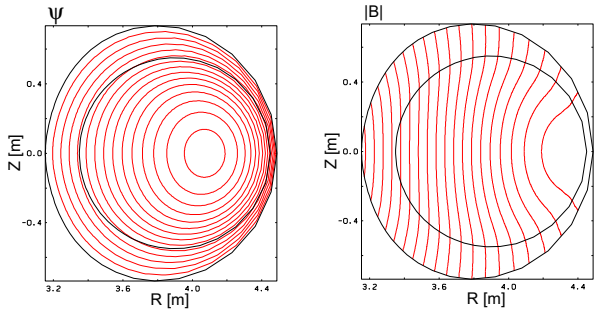

Fig. 2 Equilibrium data (A simple circular Tokamak)

Table 1 Parameters of Tokamak plasma

Plasma major radius	R_0	3.6 m
Plasma minor radius	a	0.6 m
Magnetic field at magnetic axis	B_0	3.0 T
Temperature at magnetic axis	T_0	3.0 keV
Temperature on plasma boundary	T_s	0.3 keV
Density at magnetic axis	n_0	$1.0 \times 10^{20}/\mathrm{m}^3$
Density on plasma boundary	n_s	$0.1 \times 10^{20}/\mathrm{m}^3$
Antenna current density	j_ext	1.0 A/m
Wave frequency	f_RF	42, 45 MHz
Minority ion ratio	H/D	5 %
Collisionality	ν_s	0.003

We first analyze the ICRF wave propagation and absorption in the plasma by TASK/WM. Fig. 3 are

contour plots of the real part of left circularly polarized component of the RF electric field, $\mathrm{Re}\, E_+$ (left) and the power absorption (right) on the poloidal cross section in the case of the ICRF wave frequency $f_{\mathrm{RF}} = 42\,\mathrm{MHz}$ (on axis heating). Fig. 4 are the same manner in the case of $f_{\mathrm{RF}} = 45\,\mathrm{MHz}$ (off axis heating). The ICRF waves are exited in the plasma from the antenna set on the outer side of the torus (right side). In the both cases, the $\mathrm{Re}\, E_+$ component of the waves are absorbed and the wave amplitude is damped at the minority ion cyclotron resonance layer (the minority ion cyclotron resonance layers are drawn as green lines in the left figure of Fig. 3 and 4). Then the amplitude is damped further near the two-ion-hybrid cutoff and resonance layers.

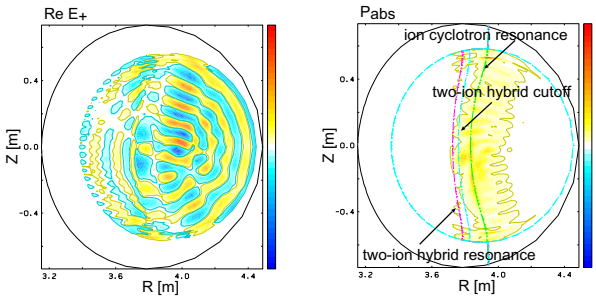

Fig. 3 Wave propagation and absorption in plasma by TASK/WM, On axis heating case ($f_{\mathrm{RF}} = 42\,\mathrm{MHz}$)

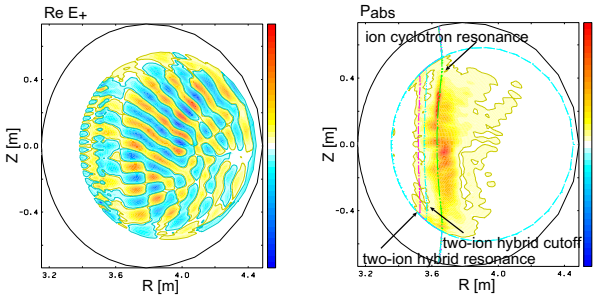

Fig. 4 Wave propagation and absorption in plasma by TASK/WM, Off axis heating case ($f_{\mathrm{RF}} = 45\,\mathrm{MHz}$)

Next, we analyzed the the evolution of velocity distribution function of minority ions and the plasma heating efficiency by GNET. The RF electric field profile obtained by TASK/WM is used to accelerate the minority ions following Eq. (6). The same plasma parameters are assumed as in the TASK/WM calculation. The test particle orbits are followed for about 0.6 s to obtain the steady state of the distribution function.

The velocity distribution function of minority ions are shown in Fig. 5 and 6. Fig. 5 are contour plots of the velocity distribution averaged on the flux surface between ρ ($= \sqrt{\psi/\psi_a}$) $= 0.0$ and 0.10 (left upper), $\rho = 0.31$ and 0.41 (right upper), and $\rho = 0.45$ and 0.55 (left lower), $\rho = 0.66$ and 0.76 (right lower) with $f_{\mathrm{RF}} = 42\,\mathrm{MHz}$ (on axis heating case). Fig. 6 shows those in the case of $f_{\mathrm{RF}} = 45\,\mathrm{MHz}$ (off axis heating case).

In the on axis heating case, the perpendicular heating by ICRF waves near the magnetic axis is observed (left upper in Fig. 5), while, in the off axis heating case, the smaller perpendicular heating near the magnetic axis is observed (left upper in Fig. 6) than that of the on axis heating case.

In these velocity distribution, the asymmetry in the parallel velocity distribution can be seen. In Fig. 5, the minority ion distribution in the positive parallel velocity region is larger than that in the negative parallel velocity region between $\rho = 0.0$ and 0.10 (left upper). Then, such asymmetry disappears in the velocity distribution between $\rho = 0.31$ and 0.41 (right upper). While, in velocity distribution between $\rho = 0.45$ and 0.55 (left lower), and $\rho = 0.67$ and 0.74 (right lower), the minority ion distribution in the negative parallel velocity region is larger than that in the positive parallel velocity region. In Fig. 6, the similar asymmetry can be seen.

In order to clarify the mechanism generating these asymmetry structure in the velocity space we study the orbit of the energetic ions. Fig. 7 shows the velocity distribution near $\rho = 0.71$ (left) and the particle orbits in the Boozer coordinates setting the parallel and perpendicular velocity marked in the left figure (right). The starting point of the poloidal angle is assume to be 22°.

It is found that the orbits show the trapped ones whose turning point are near the resonance layer. (The resonance layer becomes curved line in the Boozer coordinates.) Those particles would stay long in the resonance region and be accelerated strongly. Therefore the velocity distribution in the specific pitch angle are increased.

Also we can see the finite orbit size effect in the figure. It is observed that the particles with positive parallel velocity can be confine, while the particles with the negative parallel velocity are lost by the orbit loss, escaping from the plasma region. In this radial ρ point ($\rho = 0.71$), the distribution with the negative parallel velocity are larger than that with the positive parallel velocity. On the other hand, in the inner radial ρ point, the particles with positive parallel velocity is large. The effect of finite orbit width results in the asymmetry with respect to parallel velocity distribution of energetic particles.

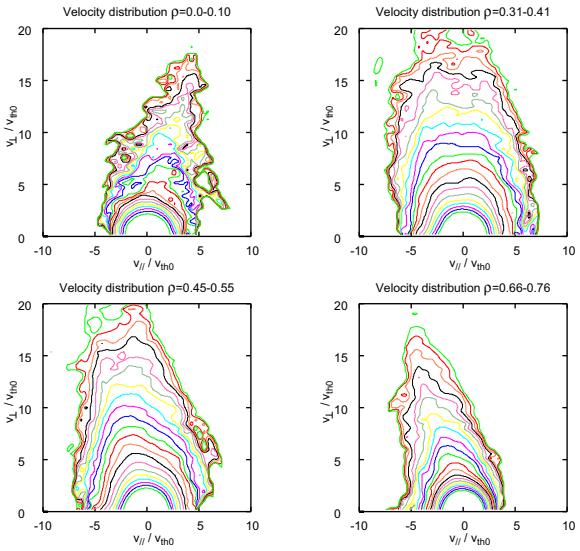

Fig. 5 Velocity distribution averaged in each radial ρ interval, On axis heating case ($f_{\mathrm{RF}} = 42\,\mathrm{MHz}$)

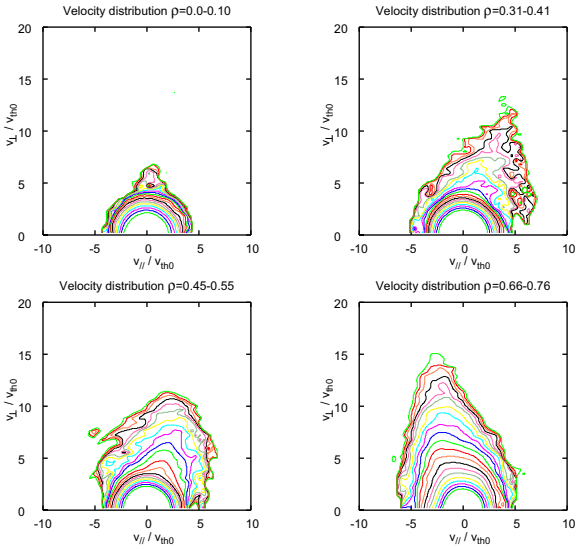

Fig. 6 Velocity distribution averaged in each radial ρ interval, Off axis heating case ($f_{\mathrm{RF}} = 45\,\mathrm{MHz}$)

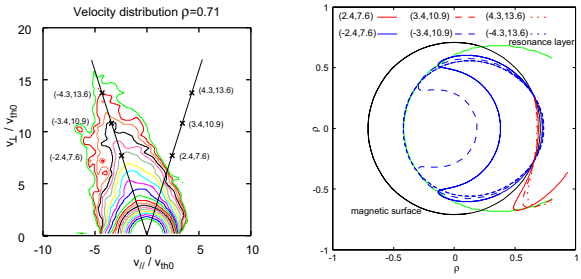

Fig. 7 Velocity distribution and particle orbit, On axis heating case ($f_{\mathrm{RF}} = 42\,\mathrm{MHz}$)

Figure 8 and 9 show the radial profile of the ICRF wave power absorbed by minority ions in the on axis heating case and off axis heating case, respectively. The left figure are results calculated by GNET and the right figure are those calculated by TASK/WM. The each radial peak positions of absorbed power calculated by GNET and TASK/WM are in good agreements. The heating efficiencies (Total heating power/Total power absorption) are 0.697 (On axis heating) and 0.396 (Off axis heating), respectively. This difference of efficiency is due to the large orbit loss in the off axis heating case.

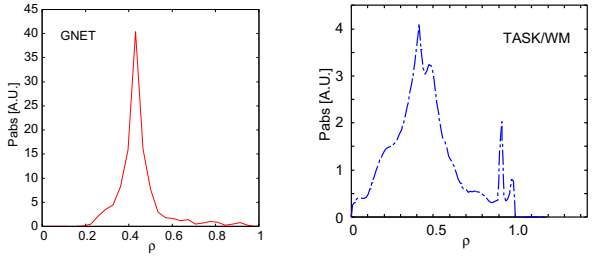

Fig. 8 Power absorption calculated by GNET (left) and TASK/WM (right), On axis heating case ($f_{\mathrm{RF}} = 42\,\mathrm{MHz}$)

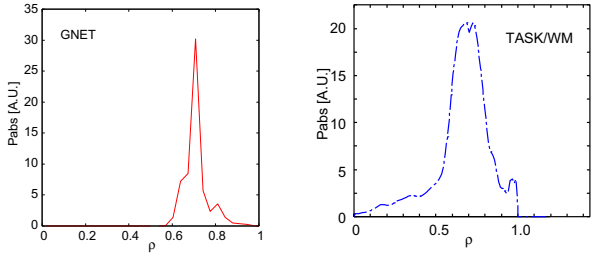

Fig. 9 Power absorption calculated by GNET (left) and TASK/WM (right), Off axis heating case ($f_{\mathrm{RF}} = 45\,\mathrm{MHz}$)

The asymmetry in the parallel velocity distribution generates the toroidal flow. We, finally, show the radial profile of toroidal velocity in Fig. 10. It is observed that the toroidal shear flow is generated by the ICRF heating because of the finite orbit width effect.

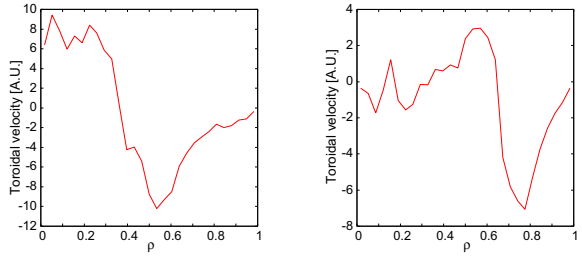

Fig. 10 Toroidal velocity, On axis heating case, $f_{\mathrm{RF}} = 42\,\mathrm{MHz}$ (left) and Off axis heating case, $f_{\mathrm{RF}} = 45\,\mathrm{MHz}$ (right)

4. Conclusion

We have been developing the global simulation code of ICRF heating combining the TASK/WM and GNET. We have carried out a global simulation of ICRF heating in a simple circular Tokamak. The realistic ICRF wave profile has been obtained by TASK/WM and has been used to solve a drift kinetic equation in the GNET.

We have found the asymmetry in the parallel velocity distribution and the asymmetry has depended on the radial position. Orbit analyses have indicated that the asymmetry arises from the finite orbit width effect of trapped particles. The asymmetry results in toroidal shear flow.

The similar code combining the Full wave code and Monte Carlo code for an axisymmetric tokamak is also developed at GA[5]. The benchmarking study of the codes is undergoing.

[1] A. Fukuyama and T. Akutsu, *Proc. 19th Int. Conf. Fusion Energy 2002*, THP3-14.
[2] S. Murakami *et al.*, Nucl. Fusion **46** (2006) S425.
[3] T. Yamamoto, S. Murakami and A. Fukuyama, Plasma and Fusion Research **3** (2008) S1075.
[4] Boozer A.H. and Kuo-Petravic G., Phys. Fluids **24** (1981) 851.
[5] M. Choi *et al.*, Phys. Plasmas 12 (2005) 072505.